Microchip gas chromatographic columns dedicated for space exploration: Stationary phase coating, setup optimization and evaluation of column performances

Arnaud Philippart, Valérie Peulon-Agasse, Malak Rizk-Bigourd, Audrey Boco-Simon, Gabin Bergerot, Guillaume Rioland, Arnaud Buch, Cyril Szopa, Pascal Cardinael

Journal of Chromatography Open 6 (2024) 100180

Contents lists available at ScienceDirect

Journal of Chromatography Open

journal homepage: www.elsevier.com/locate/jcoa

Microchip gas chromatographic columns dedicated for space exploration: Stationary phase coating, setup optimization and evaluation of column performances

Arnaud Philippart [a], Valérie Peulon-Agasse [a], Malak Rizk-Bigourd [b], Audrey Boco-Simon [b], Gabin Bergerot [a], Guillaume Rioland [c], Arnaud Buch [d], Cyril Szopa [b], Pascal Cardinael [a,*]

[a] Univ Rouen Normandie, FR3038, SMS, UR3233, F-76000 Rouen, France
[b] LATMOS/IPSL, UVSQ Université Paris-Saclay, Sorbonne Université, CNRS, 11bd d'Alembert, 78280 Guyancourt, France
[c] Centre National d'Etudes Spatiales, 31400 Toulouse, France
[d] LGPM, CentraleSupelec, Université Paris Saclay, 8-10 rue Joliot-Curie, 91190 Gif-sur-Yvette, France

ARTICLE INFO

Keywords:
Miniaturization
Microchip column
Space exploration
Stationary phase coating
Gas chromatography

ABSTRACT

This work is the first part of a project aiming to specifically design gas chromatographic microcolumns for space exploration. In particular, this study explored the functionalization and characterization of silicon/glass microchip gas chromatographic columns designed with a serpentine-shaped channel having an internal square cross-section. This microcolumn can be connected using a robust fluidic manifold with removable capillary connections to a conventional gas chromatograph or implemented in a prototype instrument for space exploration. First, benchtop gas chromatographic system was optimized in terms of injector liner volume, internal diameter (I.D.) of the capillary connections and data frequency of detection to ensure an optimal evaluation of column efficiency. Junction capillaries of 100 µm I.D., a liner of 1.2 mm I.D. and a detection acquisition frequency of 100 Hz were found to be the optimal set-up and parameters. Moreover, the stationary phase coating velocity was slowed-down to increase column efficiency by 100 %. Then, the performances of a square cross-section capillary column were compared with those of a conventional circular cross-section column. The coating efficiencies were estimated at 55 % and 42 % for circular and square internal cross-section geometries respectively, demonstrating that the square section geometry did not affect significantly the column performances. Stationary phase films of different thicknesses, from 0.032 to 0.260 µm, were coated on different microchips of the same production batch to assess the influence of film thickness on the chromatographic performances. Microchips performance was evaluated through Golay's plots, and some of the microchips were also studied by optical microscopy. The efficiency and retention capacity of our microchip column is shown to be highly dependent on the film thickness (9,000 plates.m^{-1} with $k = 0.12$ for the thinnest film and up to almost 4,000 plates.m^{-1} with $k = 0.93$ for the thickest film). Finally, the coating process repeatability was validated by producing three identical microchips with RSD of 4.8 % for the average number of theoretical plates.

1. Introduction

Gas chromatography is a powerful analytical technique that has been used for decades in the field of solar system exploration, as evidenced during the mission studying the Mars atmosphere and organic soil composition [1–3] and seeking possible traces of life. For future space missions, it is of high interest to reduce the mass of rovers and drones as much as possible to improve their flight, landing, and maneuverability capabilities, to reduce energy consumption and to access different types of environments. This reduction in payload resources requires minimizing the on-board gas chromatograph resource consumption, which starts with miniaturizing each part of the gas chromatograph, *i.e.* the injection system, the column, the detector and the electronic (but not part of this study). Interest in miniaturizing gas chromatography columns has grown considerably in recent years with the emergence of microchip columns based on MEMS (Micro Electro Mechanical System) technology. In 2018, a review about the state-of-the-art for such columns was published [4] presenting a column classification in terms of

* Corresponding author at: Université de Rouen Normandie, SMS UR3233, Emile Blondel 76821 Mon-Saint-Aignan Cedex, France.
E-mail address: pascal.cardinael@univ-rouen.fr (P. Cardinael).

https://doi.org/10.1016/j.jcoa.2024.100180
Received 23 July 2024; Received in revised form 21 September 2024; Accepted 23 September 2024
Available online 5 October 2024

coating, column geometry, column dimensions, column interface, and performances. Other reviews reported the advances in gas chromatograph microdevice research, component by component, from the injector to the detector, and showed the complexity of integrating such components together [5–7]. Another review focused on the variety of stationary phases coated on microchip columns [8–9], and the two main microchip channel geometries (serpentine and spiral) were compared [10]. Several microchip designs and functionalization methods have been reported in the literature [5–7,10–11]. Different studies have explored various materials and supports for stationary phase preparation [12–14]. According to these works [7,10–11], efficiency values for mono-channel microchip coated with polydimethylsiloxane (PDMS) in isothermal conditions were ranged from 2193 to 17,500 theoretical plates, depending on shape design and geometry of the microcolumns. The reason why microchip columns do not have the same performance as conventional columns might be due to the microchip design and channel geometry, which could disrupt the gas flow and/or the ability to coat a homogeneous film. In particular, most of the cross-section channels are square ones, which can make the coating of the stationary phase film more heterogenous because the right angles are less accessible to it than the rest of the surface or on the contrary the right angles could pool the stationary phase on the channel corner. Therefore, homogeneous films could be much more difficult to coat onto the inner wall of columns containing square channels compared to cylindrical columns. In addition, serpentine-shaped columns affect the carrier gas flow and pressure distribution [10]. Concerning, the microchip substrates, they are mainly micromachined in silicon wafers with a top cover made in glass, and this material difference can be a source of heterogeneity in the stationary phase coating depending of the wettability of the surfaces. Finally, most microchip setups have high temperature limitations, which constrain efficient deactivation and other chemical treatment steps as well as the analysis of low volatile compounds.

In the field of space exploration, a research team developed MEMS columns and used them in experimental GC prototype coupled to a MS for the analysis of organic molecules in space environments [15–17]. In their works, the column chips were designed with fluidic inlet and outlet positioned laterally on the chip side, and the connections to the other parts of the GC were usually done using capillary tubes fixed with adhesives or epoxy glue. Considering space instrumentation constraints, this design is not mechanically the most robust and not well-suited to space applications. To our knowledge, only one study [18] reported a metal box, metal nuts and graphite ferrules for interfacing the column with the other components, but the whole set-up does not meet mechanical constraints of space instrumentation because a major component is made of glass.

In this context, our teams are involved for more than eight years in the development of MEMS columns designed for space exploration with fluidic inlet and outlet drilled in the upper part of the chip. This fluidic design allows a more robust integration of the column onto a fluidic interface based on a patented design [19] suited to space instrumental constraints. GC systems based on MEMS technology for space exploration can allow a jump of scale in system dimensions, weight, and power consumption. Moreover, this technology should remain mechanically robust. The fluidic interface is based on the use of screwed connections with capillaries that can be easily changed in case of clogging without damaging the microchip column. The dead volume was optimized and is <1 µL to preserve the column efficiency. Nevertheless, this interface is limited to a maximum temperature of 150 °C due to the use of a gas-tight seal made of a polymer (Tefzel).

Thus, the main objective of this work was to develop and optimize a method for stationary phase coating on microchips implemented in this fluidic manifold specifically designed to space exploration [19,20] and considering its temperature limit. The experimental chromatographic setup (*i.e.* the manifold used with the column microchip connected with capillaries to the injector and detector of a commercial GC) was optimized to evaluate the most representative performance for the microchip, and to determine the influence of each part of the set-up (from the injector to the detector) contributing to extra-column volumes. Then, chromatographic column performances were compared using the optimized manifold and calculating the coating efficiency. In addition, a discussion about the influence on stationary coating of square cross-section columns compared to circular cross-section columns (conventional columns) was provided.

2. Material

2.1. Microchips, fluidic interface and capillaries junction

The square cross-section channel columns (microchips) used in this study were fabricated by ESIEE (École Supérieure d'Ingénieurs en Électrotechnique et Électronique, Paris) and were based on MEMS technology. These microchips (3.5 × 3 cm) were micromachined in silicon substrates with a square cross-section channel etched by photolithography and plasma ion collision (deep reactive-ion etching) and then covered with a Borofloat® glass plate (SiO_2 81 %, B_2O_3 13 %, Na_2O/K_2O 4 %, Al_2O_3 2 %). All microchip channels were 5 m long, and the square cross-section was 115 × 115 µm, resulting in a column volume of 66 µL. Microchip surface oxidation allowed the formation of an oxidated layer of 200 nm for the two batches of microchips used. The fluidic inlet and outlet were perpendicular to the microchip (through the channels). A schematic representation and a picture of the column are shown in Fig. 1, and a X-ray tomography 3D image is shown in Fig. 2. X-ray tomography images were recorded on an EasyTom160 instrument from RX Solutions (Chavanod, France) using a voltage of 100 kV and a current of 100 µA.

The microchip was integrated during the coating process and chromatographic tests, onto the fluidic manifold designed and fabricated by LATMOS (Laboratoire Atmosphères et Observations Spatiales, Guyancourt). The manifold design is based on a patented manifold used for a prototype of space GC (Fig. 3) [16]. The inlet and outlet connections on the fluidic interface were done using silica capillaries for deactivation and coating steps and polyetheretherketone (PEEK) (25 cm long, 100 µm internal diameter I.D.) for the chromatographic tests. Commercially PEEK nuts supplied from VICI company and gas-tight seals (Tefzel) were used to ensure airtight connections.

2.2. Gas chromatograph

Chromatographic analyses were performed on Agilent 7890B gas chromatograph equipped with a split/splitless injector, an Agilent G4513A autosampler and a flame ionization detector (FID) (300 mL.min^{-1} of air, 30 mL.min^{-1} of H_2 and 10 mL.min^{-1} of N_2 for makeup). For the chromatographic tests, the injection volume was set at 0.1 µL. Different detector acquisition frequencies were tested between 10 and 200 Hz). The carrier gas was selected as H_2 (supplied by Air Liquide, Paris) at a purity of 99.995 % to minimize the column pressure drop and reach a higher optimal velocity. The temperatures of the injector and the detector were set at a maximum of 200 °C for PEEK junction capillaries and 250 °C for fused silica capillaries. Chromatograms were acquired with Agilent OpenLAB software but were reprocessed with Chromeleon (version 7.2.10) after exporting the AIA file.

2.3. Chemicals

1,1,1,3,3,3-hexamethyldisilazane (HMDS), *N*-(trimethylsilyl)imidazole, *N,N*-dimethyltrimethylsilylamine (TMSDMA), methyltriethoxysilane (MTEOS), *2,2,4*-trimethylpentane (isooctane), methanol and diethyl ether were purchased from Acros Organics (Morris Plains, New Jersey, USA). Pentane and dichloromethane were obtained from VWR International (West Chester, USA). Hydrochloric acid (HCl) and trifluoroacetic acid (TFA) were purchased from Fisher Chemical (Waltham, Massachusetts, USA). OV-1 (PDMS) was purchased from MEGA

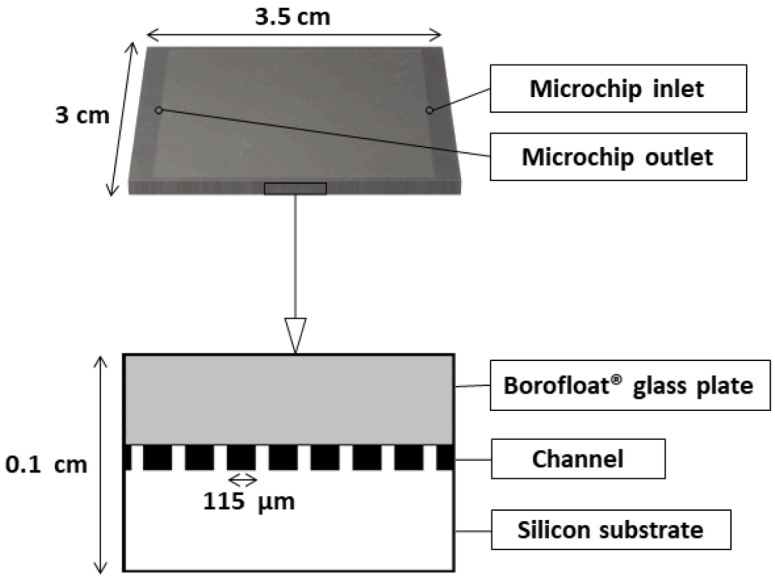

Fig. 1. Schematic representation of the microchips used with a view of the cross-section (top). Picture of the microchip from above (bottom).

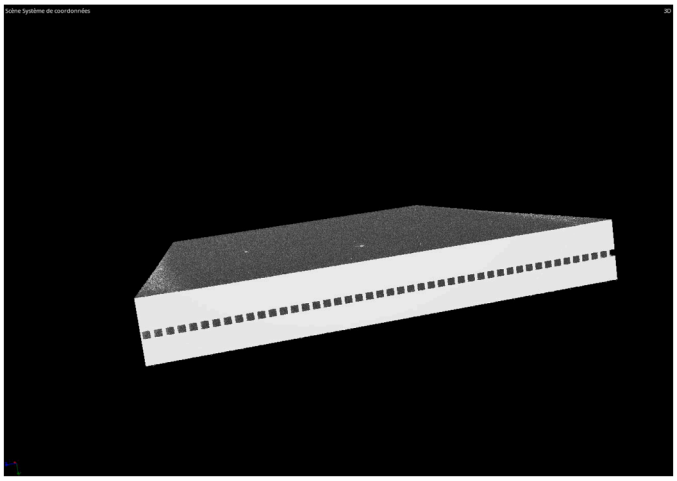

Fig. 2. 3D image of the microchip section. This image was provided by the CNES (Centre National d'Etudes Spatiales, Toulouse, France) using X-ray tomography instrument.

(Legnano, Italy). Polyethylene glycol (PEG) 20 M was purchased from Ohio Valley Specialty Company (Marietta, United States). Silica tubes were provided by MicroQuartz (Munich, Germany).

2.4. Other materials

Channel visualization was carried out using a Nikon Eclipse LV100 microscope equipped with a Nikon Digital Sight DS-Ri1 camera. Images were analyzed using NIS-Elements D 3.1 software.

The precision balance used for stationary phase solution preparation was a Sartorius BP 210 S. The nanobaume used for stationary phase coating was connected to the inlet of the manifold via a FEP (fluorinated ethylene propylene) tube, a 0.2 µm inox filter and a fused silica capillary. The syringe pump used for silanization was an AL-1000 from World Precision Instruments.

3. Method

3.1. Stationary phase coating

The static coating method was selected because this process is well known in our team [21] and allows controlling the film thickness (d_f) as commonly be used for microchips [22–24] and provides better efficiencies than the dynamic method [9,25]. This method adapted for the use of microchip with the manifold developed for space application was patented [16].

First, the microchip was deactivated with HMDS at 150 °C for 24 h using a dynamic method established for chemical treatment of microchips at low temperature. For the coating, the microchip was filled with a solution of PDMS in a dichloromethane/pentane 50/50 v/v mixture. Stationary phase solutions were prepared by weighing a precise mass of

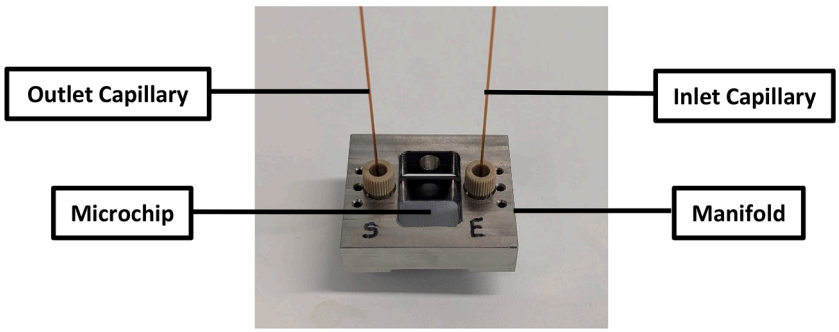

Fig. 3. Picture of the manifold and the junction capillaries.

polymer and dissolving it in the solvent mixture. The solution was then ultrasonicated until complete dissolution of the polymer. The solution was then filtered through a 0.2 µm PTFE (polytetrafluoroethylene) filter. The film thickness was directly related to the polymer concentration according to Eq. (1).

$$df = \frac{C_{SP} \times I.D.}{4 \times \rho_{SP}} \quad (1)$$

where ϱ_{SP} is the polymer density (1 g.cm^{-3} for PDMS), C_{SP} is the polymer concentration and I.D. is the internal diameter of column.

The stationary phase used in this study is the PDMS because it is a nonpolar phase usually used for space GCs [26–28]. Moreover, PDMS stationary phases have already been used for microchip coating [8,11, 29–31] and are known to have good chemical inertness, high thermal stability and film homogeneity.

The microchip filling was performed using a nanobaume and N_2 to push the stationary phase solution into the microchip. Once the microchip was completely filled, the outlet tube was sealed with a septum, and the manifold was connected to a vacuum pump for solvent evaporation at a fixed reduced pressure (4 mbar or 400 mbar) and within a water bath set at 20 °C. The removal of the solvent led to the stationary phase coating onto the microchip internal surfaces. After a final step of 12 h of thermal maturation at 150 °C (rising to 1 °C.min^{-1}), the microchip was ready for testing.

3.2. Chromatographic system and experimental condition optimization

Chromatograph system and experimental conditions should be optimized because the microchip volume is reduced compared to conventional columns, and the microchip junction capillaries have additional and extra-column volumes must be considered. Furthermore, the injection volume must be reduced as much as possible while ensuring injection efficiency and repeatability [32]. Each analytical module including fluidic interface, junction capillaries, GC inlet and GC detector parameters, were optimized to reduce the loss of performance due to extra-column dispersion.

The fluidic interface with the lowest dead-volume was designed to limit extra-column variance. This volume was <1 µL and was negligible compared to the 66 µL microchip volume. For each batch comparison (each batch contains 3 tested columns), only the microchip was removed from the manifold and replaced, and the other parts of the analytical systems (liner, capillaries) were kept identical to ensure the reliability of the comparison. The column performances were measured with a classic liner (4.0 mm ID) and compared to those obtained with a thinner liner (1.2 mm ID) in order to limit the variance due to the injection. The split ratio was set at 1:100 to limit the sample volume transferred into the microchip (the lower injection pulse) while ensuring injection repeatability. A comparison of different FID acquisition frequencies was also achieved, and the optimal frequency was set to 100 Hz to obtain a sufficient number of data points to correctly define the peak shape while avoiding a decrease in sensitivity and a larger amount of data. Then, the influence of junction capillary I.D. on efficiency was studied. For this part, PEEK capillaries of 50, 100 and 250 µm I.D. were connected to the fluidic interface with an uncoated microchip. For each diameter tested, both capillaries connected to the fluidic inlet and outlet were 25 cm long. Microchip efficiencies were measured by plotting Golay's plots (Eq. 2) obtained by three injections of 0.1 µL of *2,2,4*-trimethylpentane (isooctane) with a 1:100 split ratio at 100 °C, and using different linear gas velocities (µ) from 15 to 130 cm.s^{-1}.

$$H = B/\mu(C)\mu \quad (2)$$

H is the height equivalent to a theoretical plate, B the longitudinal diffusion and C is the mass transfer term. H_{min} is defined as the plate height at the Golay's plot minimum.

The efficiencies were evaluated by the calculation of the number of theoretical plates (N) from Eq. (3):

$$N = 5.54(tr/wh)2 \quad (3)$$

with w_h the peak width at half height and t_r the retention time. All microchip retention factors given were measured at 100 °C.

All microchip retention factors (k) were calculated using Eq. (4):

$$k = \frac{(t_R - t_0)}{t_0} \quad (4)$$

with t_0 the retention time of a non-retained compound (*n*-butane).

3.3. Square/circular cross-section column comparison

To estimate the possible performance losses induced by the square cross-section shape, a comparison between square and circular cross-section capillary silica columns was carried out using a 5-meter silica tube for both section shapes. The circular tube I.D. was 100 µm, and the square tube section was 100 × 100 µm. Stationary phase coating on both tubes was performed following strictly similar protocols (described in Section 3.1) with a PDMS concentration of 4 g.L^{-1}. Film thickness was estimated using Eq. (1) and the nominal channel inner diameter (nd_c) for the square cross-section which was calculated through the following Eq. (5) [33]:

$$ndc = 2(S/\pi)1/2 \quad (5)$$

where *S* is the area of the channel section.

The film thickness was estimated at 0.115 µm and 0.1 µm for the square cross-section column and the circular cross-section column respectively.

Efficiencies were compared by plotting the Golay's plots with data measured by the injection of isooctane. The retention factors were calculated by injection of isooctane and butane. All the other chromatographic conditions are described in Section 3.2. The isooctane was selected because was already used to evaluate column performances as quasi non-retained compounds [21,34].

3.4. Microchip coating evaluation

Three microchip batches were used to evaluate the success of microchip coating. First, the influence of the coating rate (solvent evaporation rate) on the film homogeneity and efficiency was studied. With this aim, two microchips from the same batch were prepared while varying the pressure of the vacuum pump, to allow solvent evaporation from 4 mbar to 400 mbar. Microchips were functionalized with a 4 g.L^{-1} PDMS solution resulting in a film thickness of 0.130 µm, while keeping all other conditions unchanged. Secondly, the influence of the film thickness on chromatographic performances (efficiency and retention) was studied. For this purpose, three microchips from the same batch were prepared while varying the PDMS concentration from 1 to 8 g.L^{-1} to have different film thicknesses from 0.032 to 0.260 µm. Finally, the repeatability of microchip coating was investigated by preparing three microchips from the same batch with a PDMS concentration of 8 g.L^{-1}, resulting in a film thickness of 0.260 µm. Chromatographic measurements were performed according to the chromatographic conditions described in the result section. Some coatings were also observed by optical microscopy, and the channels were photographed.

It should be noted that the comparison of microchips from different batches may introduce some variability because each batch is manufactured separately, which may cause slight differences in the channel surface state. Manufacturing constraints do not allow all columns to be produced in one batch but all batches were visually controlled by ESIEE after manufacturing.

4. Results and discussion

4.1. Chromatographic system and experimental condition optimization

4.1.1. Selection of the internal diameter of the injection liner

The results obtained with the two liners tested are shown in Table 1, and the corresponding chromatograms are shown in Fig. 4. The smaller liner volume limited the gas diffusion generated during the injection, resulting in less band broadening and therefore a better chromatographic efficiency. However, it is important to inject very small amounts to ensure that the volume of gas generated does not exceed the liner volume. In addition, the retention time was shifted and reduced for the thinner liner (1.2 mm), because the analytes stay less longer in the liner (the gas velocity on the thinner liner was increased due to its lower volume, so the retention time was slightly decreased). The area measurements ensured that the amounts vaporized in the liner and injected into the microchip were similar. Thus, a liner of 1.2 mm I.D. was used for the remainder of the analyses performed in this work.

4.1.2. Selection of the data acquisition frequency

The results for each data acquisition frequency tested from 10 to 200 Hz are listed in Table 2, and the corresponding chromatograms are shown in Fig. 5. It is worth noting that, it was not possible to access to the time constant of the detector which affects the efficiency. These results showed that chromatographic efficiency was improved significantly with increasing data acquisition frequency. However, the peak broadening and thus the efficiency gain from 100 Hz to 200 Hz remained negligible and produced a larger data volume, which is preferable to limit in the context of miniaturization and space exploration. Thus, a data acquisition frequency of 100 Hz was used for the remaining analyses performed in this work.

4.1.3. Selection of junction capillaries internal diameter

Fig. 6 shows a comparison of Golay's plots using inlet and outlet PEEK capillary connections with different I.D. (liner I.D. and data acquisition frequency were 1.2 mm and 100 Hz, respectively). The plot comparison showed that reducing the I.D. of the capillaries from 250 µm to 100 µm improved the efficiency, which was expected since the extra-column variance was reduced. Furthermore, with 50 µm I.D. capillary connections, the resulting pressure drop prevented us from exploring the highest linear velocities to clearly determine the corresponding profile and then the analyte diffusion (C) value. Nevertheless, H_{min} appeared higher than that obtained with the 100 µm I.D. junctions. It can be assumed that when the internal diameters of junction capillaries and microchips were similar (≈100 µm), the best efficiency was obtained. In this case, a uniform gradient of pressure (and thus the velocity) was maintained along the entire system. Thus, any funnel effect was observed. With 50 µm I.D. capillaries, the velocity was limited by the pressure drop despite the use of dihydrogen as carrier gas. Thus, 100 µm I.D. capillaries were selected for the following analyses as their I.D. was close to the internal diameter of the microchip channel.

Table 1
Comparison of isooctane peak efficiency as a function of the tested liner I.D. The data acquisition frequency, junction capillary I.D. and injected volume were 100 Hz, 100 µm and 0.1 µL, respectively.

Liner I.D. (mm)	Liner volume (µL)	Peak area (pA.min)	Half height width (min)	Number of theoretical plates
4.0	990	41.4	0.0057	5150
1.2	90	44.3	0.0032	14,450

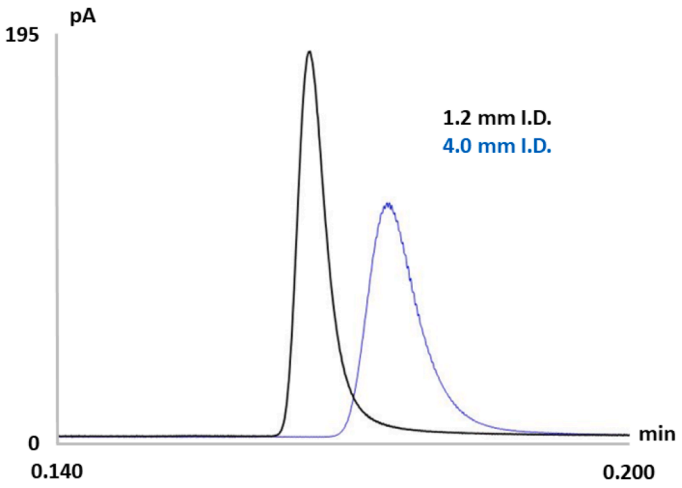

Fig. 4. Chromatograms obtained by the injection of isooctane at 100 °C according to the conditions specified in the method with the liner of 1.2 mm I.D. (in black) and the liner of 4.0 mm I.D. (in blue).

Table 2
Comparison of isooctane peak efficiency as a function of data acquisition frequency. Liner I.D. and connection capillary I.D. are 1.2 mm and 100 µm, respectively.

Acquisition frequency (Hz)	Half height width (min)	Number of theoretical plates
10	0.00567	4780
20	0.00395	9770
100	0.00328	14,180
200	0.00320	14,920

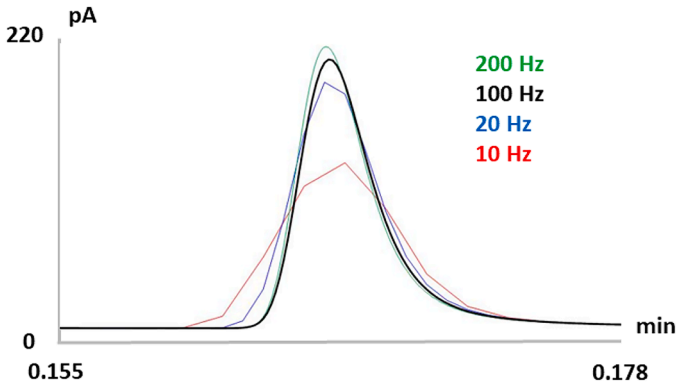

Fig. 5. Chromatographic profiles obtained by the injection of isooctane according to conditions specified in the method and using the following data frequency acquisition (red) 10 Hz, (blue) 20 Hz, (black) 100 Hz and (green) 200 Hz.

4.2. Square/circular cross-section comparison

Experimental Golay's plots obtained for capillary tubes with circular and square internal cross-section geometries are shown in Fig. 7. As expected, the minimum H value, *i.e.* 70 µm, was obtained for the circular cross-section of 100 µm I.D., while the square cross-section was less efficient, with a minimum H value of 107 µm for a nd_c of 115 µm. The retention factors calculated for isooctane on both tubes were similar (0.19 and 0.18), indicating that the amount of coated stationary phase was almost the same for both columns. The coating efficiency (E%) can be estimated by using the Eq. (6):

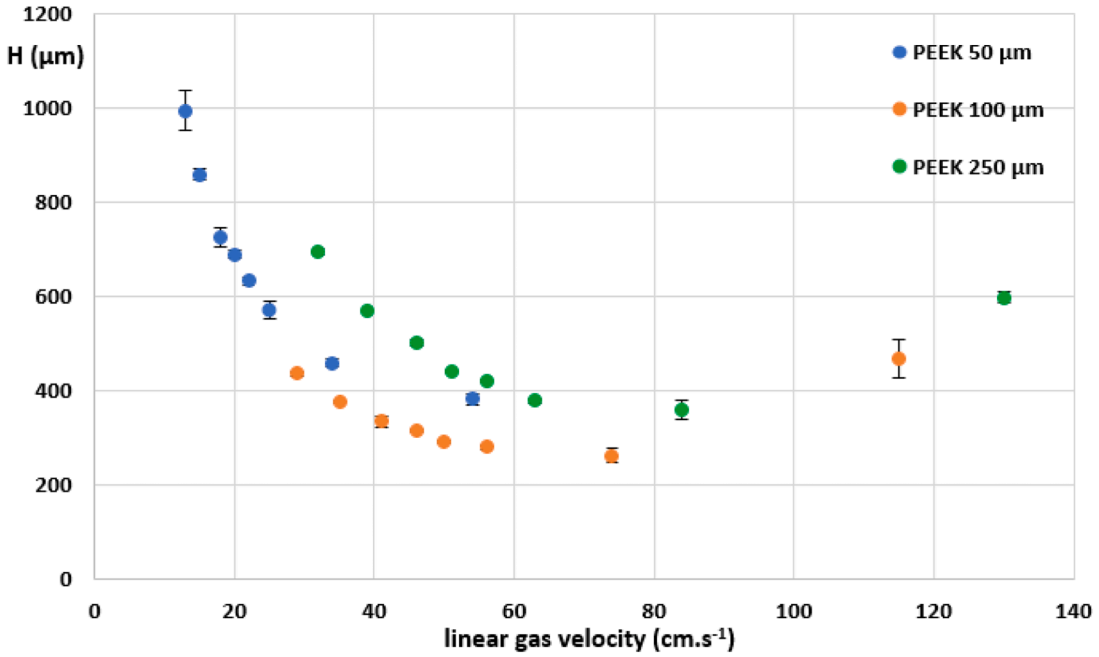

Fig. 6. Evolution of H *versus* the mean linear carrier gas velocity for all the junction capillaries tested by the injection of isooctane at 100 °C in triplicate with the corresponding RSD.

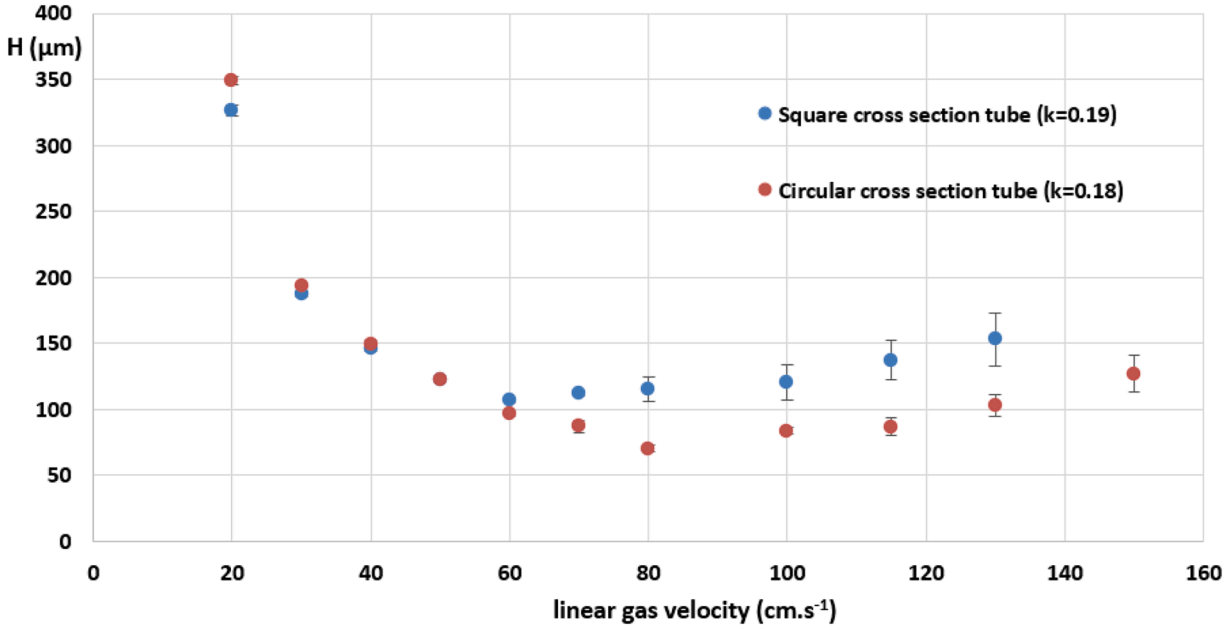

Fig. 7. Comparison of Golay plots of circular and square cross-section tubes coated with PDMS film obtained by the injection of isooctane at 100 °C in triplicate (RSD on H values for each velocity were <5 %).

$$E\,\% = \frac{H_{theoretical}}{H_{experimental}} \times 100 \quad (6)$$

With H_{min} was deduced from Golay's plot and $H_{theoretical}$ was estimated using the Eq. (7):

$$H_{theoretical} = r\sqrt{\frac{1+6k+11k^2}{3\ \times (1+k)^2}} \quad (7)$$

Where r is the internal radius of the column.

It should be noted that there is a slight difference of surface between the circular section (100 µm I.D.) and the square section (100 × 100 µm corresponding to a nd_c of 115 µm) and so the film thicknesses were 0.1 µm for the circular section and 0.115 µm for the square cross section. Consequently, the coating efficiencies were estimated to be 55 % and 42 % for the circular and square internal cross-section geometries respectively, demonstrating that the square section geometry slightly affected the coating efficiency compared to the conventional circular cross-section.

The determination of C term was estimated by a graphical estimation using an in-house Excel program developed in-house. Moreover, the C term values were different and were estimated to be 1.3×10^{-4} s for the circular cross-section and 1.6×10^{-4} s for the square cross-section. Since

the retention factors were similar, the higher C term value obtained for the square cross-section tube could be attributed to a difference of film homogeneity and/or film thickness.

4.3. Influence of the coating rate

In this part, two reduced pressured (4 mbar and 400 mbar) were applied to the vacuum pump to generate two different microchip coating rates. Chromatographic measurements and optical microscopy were performed to evaluate the influence of the coating rate on the film homogeneity.

4.3.1. Reduced pressure for column coating

Table 3 shows that a reduced pressure set at 400 mbar during the stationary phase coating allowed a better efficiency than a pressure set at 4 mbar according to the obtained number of theoretical plates. Reducing the coating speed of the stationary phase by slowing down the evaporation rate seems to reduce the coating heterogeneity. The similar retention factors obtained for microchips 1 and 2 indicated that the amount of coated PDMS was similar. So, the difference of efficiency can be attributed to the coating quality.

4.3.2. Optical microscopy observations

Optical microscopy was used to investigate the PDMS coating inside the microchip channels. Three areas of the channel were observed (Fig. 8): the "microchip part near inlet", the "microchip middle part" and the "microchip part near outlet".

Images (Fig. 9) showed that the PDMS coating on microchip 1 was heterogeneous. Fig. 9(a, c and e) showed clearly the presence of PDMS droplets on the silicon surface, while the appearance of the coating was different on the glass surface (pictures 9 (b) and (d), where the droplet sizes were smaller. This difference may simply be explained by the difference in the wettability of both surfaces (silicon and glass) towards the PDMS, and the deactivation reaction may also be different between both materials. Likewise, differences were observed among the three observed parts of the microchip. The droplet diameter decreased until disappearing from the inlet to the outlet of the microchip, suggesting that the coating was better at the end of the microchip where the evaporation has slowed down.

Optical microscopy images obtained on the microchip 2 (Fig. 10) show similar results. The coating of the microchip part near the inlet was heterogeneous with many cracks along the glass side (Fig. 10a) while, the coating of the microchip middle part has a better appearance with cracks along only one direction on the glass side (Fig. 10b). Finally, the coating of the microchip part near the outlet was homogeneous, (Fig. 10c). These results confirm the previous observation done on the microchip 1 and the evolution of the coating quality as a function of the location within the microchip channels.

Experimentally, evaporation is faster at the beginning of the microchip and is slowed down gradually due to the distance from vacuum pump. The observed film cracking can be explained by the fact that the pooling of polymer could occur at the right-angle of the channel and the coated film may be broken or form stationary phase droplets due to a bad wettability of the surface towards PDMS.

Overall, it seems that the control of the evaporation rate during the static coating method and reducing it was very important. The microchip 2 coating obtained with solvent evaporation at 400 mbar was much more homogeneous than the microchip 1 coating. Reducing the coating rate was beneficial and limited droplet formation. The difference in the PDMS affinity for both surfaces (silicon and glass) could explain the differences in droplet size observed on both materials. Furthermore, both microchip coatings appeared to be better near the outlet than at the inlet especially on the glass surface due to the coating rate evolution. To overcome this problem, the reduced pressure could be controlled during the evaporation in order to keep it slow and constant during the whole process. However, it is technically difficult to adjust manually the pressure and this regulation was not performed during this study.

Table 3
Theoretical plate numbers and retention factors as a function of the solvent evaporation rate controlled by the reduces pressure set at 400 mbar and 4 mbar. The carrier gas velocity was set at 60 cm.s^{-1}. Values of width at half height and efficiency were the average values obtained over 3 injections of isooctane at 80 °C, and the RSD values are provided in brackets.

Microchip Number	Reduced pressure (mbar)	Retention factor (*k*) isooctane	Number of theoretical plates
1	4	0.30	11,500 (0.7 %)
2	400	0.26	21,000 (3.0 %)

4.4. Influence of the stationary phase film thickness

For this part of the work, three microchips from the same production batch, called in the following microchip 3, 4 and 5, were coated with three different film thicknesses. The maximal efficiencies shown on the Golay's plots (Fig. 11) for each film thickness tested are listed in Table 4, and the graphical estimation of the B and C terms of the Golay's plots is presented in Table 5.

The results in Table 4 show that the efficiency increased with decreasing the film thickness, and an efficiency of 45,900 theoretical plates was obtained for the thinnest film which was an excellent result for mono-channel micro-columns compared to the literature [4–8,11]. Nevertheless, when a more concentrated solutions were injected or the split ratio was decreased, an overloading of the stationary phase quickly occurred (peak fronting). The retention factors (*k*) calculated for isooctane injection at 80 °C were proportional to the film thickness. These results indicated that our microchip functionalization method was consistent and reliable. As expected, the best coating efficiency (42 %) was obtained for the thinnest stationary film. The coating efficiency observed for square cross section capillary column was 42 % comparing to 35 % for microchip with comparable film thicknesses. This result could be explained by the serpentine design leading to heterogeneity in gas velocity [10] and/or the presence of glass surface for the microchip.

The calculated B and C terms were graphically estimated. The C terms values increased with the film thickness, as theoretically expected. Additionally, the C term value observed for microchip 4 was similar to the C term value obtained for the square cross-section tube (Section 4.2). As microchip 4 and the square cross-section tube tested have similar geometric parameters (115 × 115 µm *versus*100 × 100 µm) and were functionalized with the same protocol and the same amount of stationary phase, this result was expected. The longitudinal diffusion (B term), specific to the compound diffusion in the gas phase, was constant.

In comparison to commercially available cylindrical open tubular columns, having a number of theoretical plates per meter varying approximately from 7300 to 12,500 (internal diameter I.D. =0.1 mm) and from 4000 to 6600 (I.D.=0.18 mm), our column presented a value varying between 3980 and 9180 which was consistent and promising for *in-situ* space applications. In this field, only a recent study on experimental MEMS GC developed for space environments [13] reported an average number of theoretical plates of 1624 per meter over the column temperature range of the separation. Therefore, the average number of theoretical plates per meter for our tested column is 2.4 to 5.6 times. Nonetheless, microchip GC column technology is not yet standardized or commercialized. It is still under development and the current literature is replete with various column geometries and different cross section parameters. Besides, the test temperature conditions, the setup used (injection system, extra-column tube volumes), the nature of analytes and the nature of stationary coating (static or dynamic) are to consider in the comparison of columns efficiency and any direct comparison is not obvious and sometimes irrelevant. Nevertheless, a microchip exhibiting about 45,000 theoretical plates in isothermal conditions was

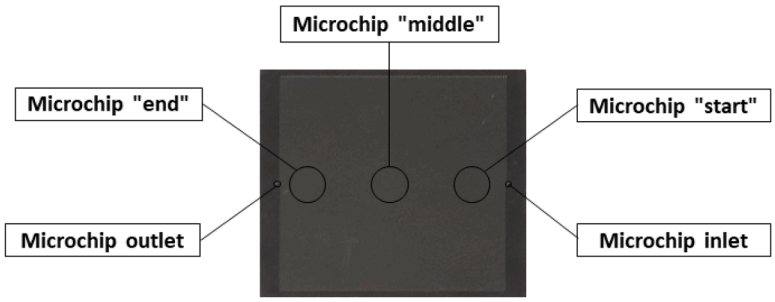

Fig. 8. Photograph of the microchips used with the different investigated zones.

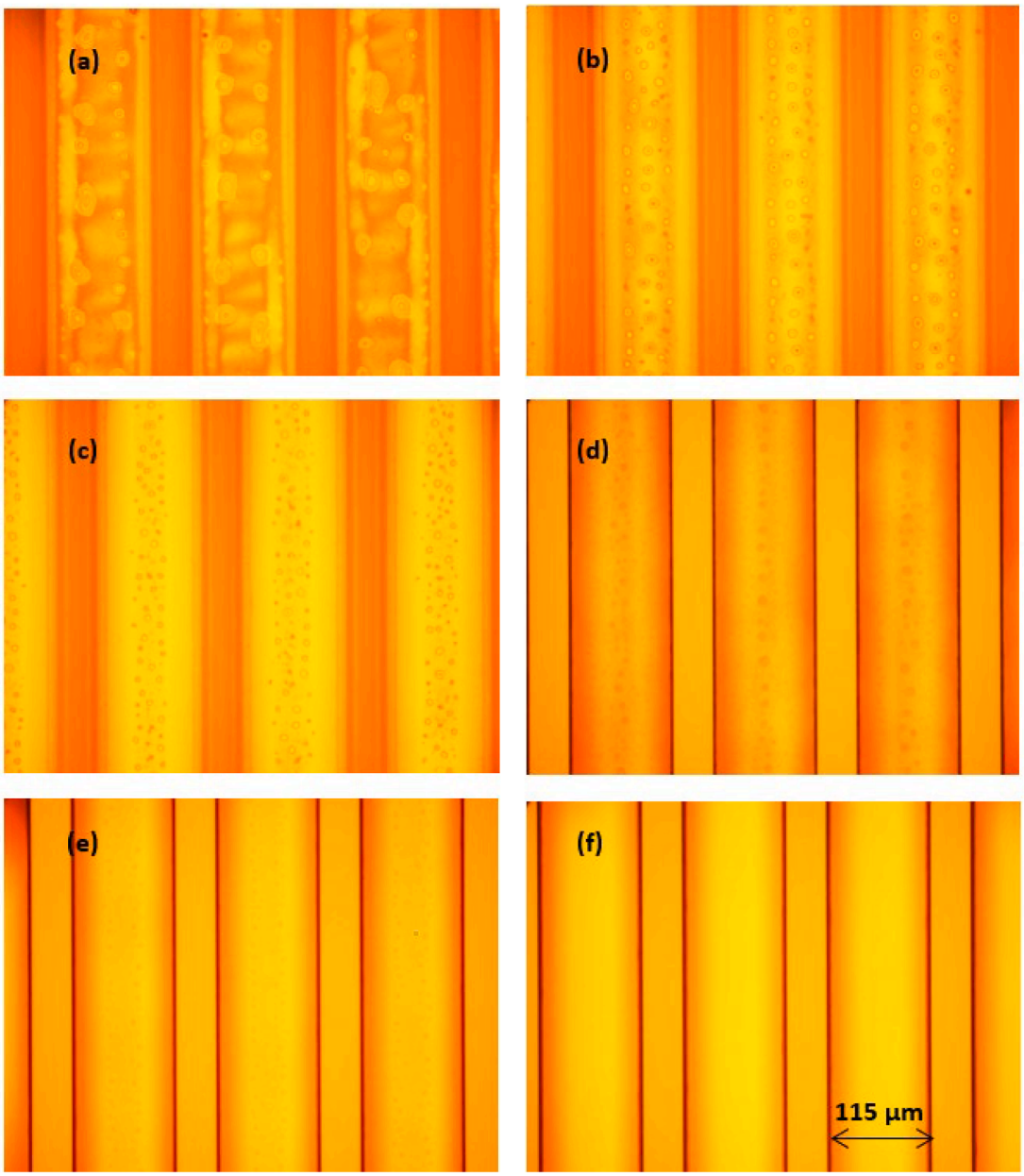

Fig. 9. Optical microscope pictures obtained for microchip 1. (a) lower surface start (silicon), (b) upper surface start (glass), (c) lower surface middle (silicon), (d) upper surface middle (glass), (e) lower surface (silicon) end, and (f) upper surface end (glass) of the microchip.

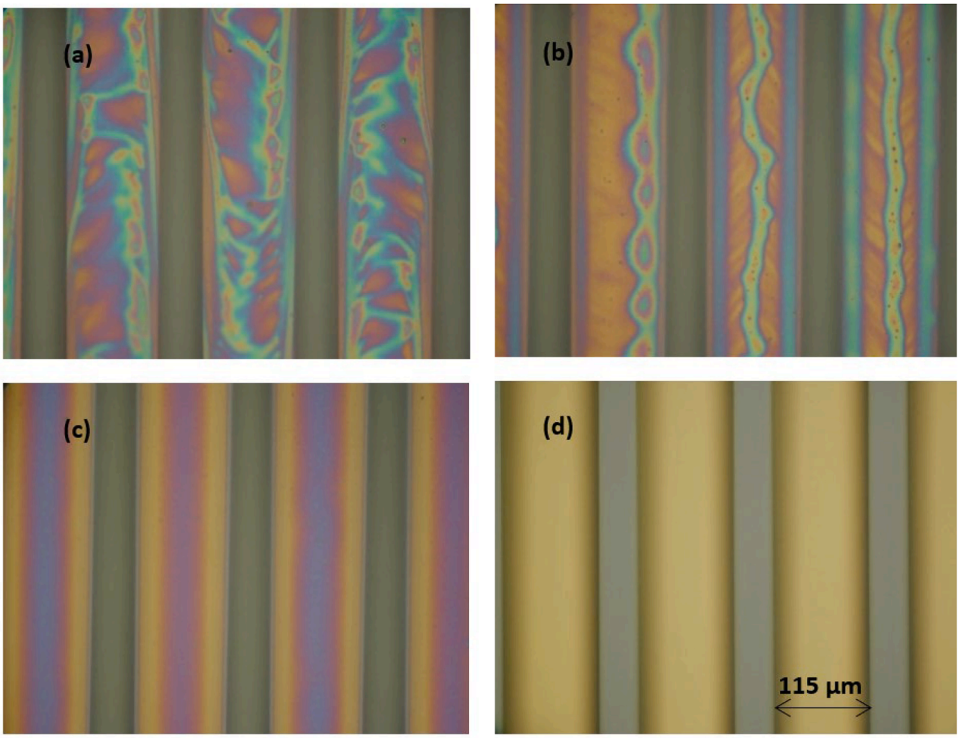

Fig. 10. Optical microscope pictures obtained for microchip 2. (a) upper surface start (silicon), (b) lower surface middle (silicon), and (c) upper surface end (silicon) of the microchip and an (d) upper surface uncoated microchip.

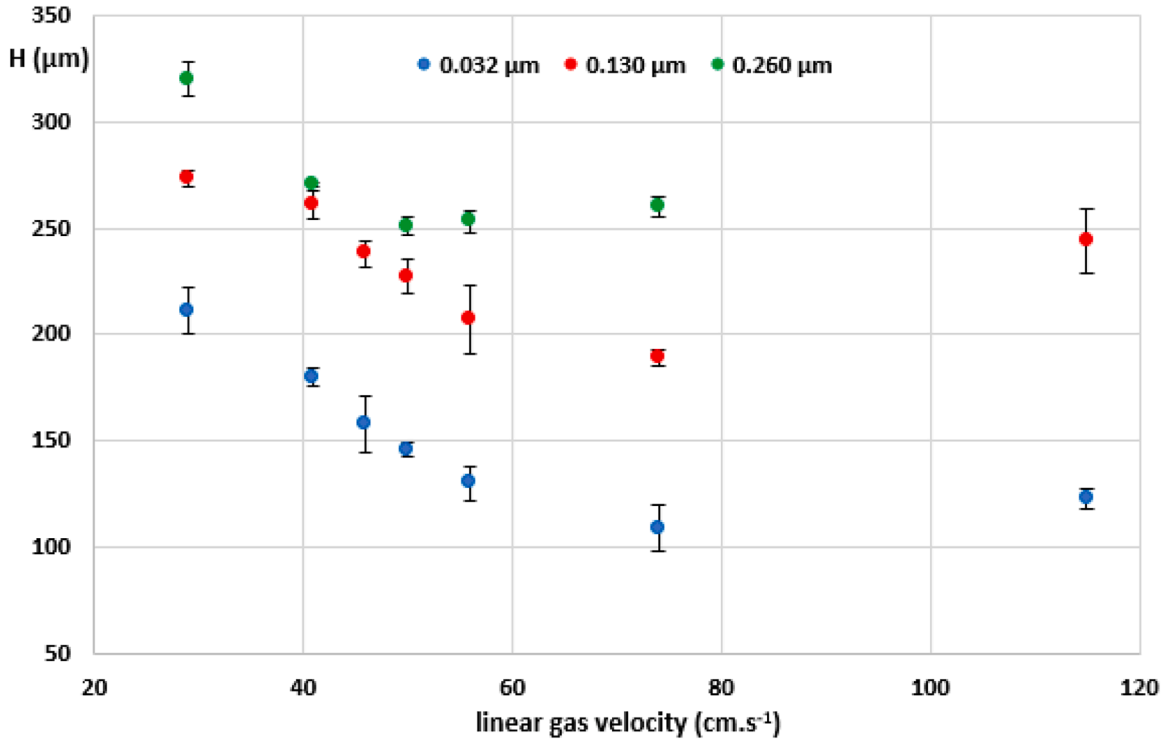

Fig. 11. Golay's plots of the three microchips detailed in Table 5 obtained by the injection of isooctane at 100 °C in triplicate (RSD on H values for each velocity were <10 %) d. Each curve corresponds to a PDMS film thickness.

an excellent result for mono-channel micro-columns compared to the literature [4–8,11]

4.5. *Coating repeatability*

Three microchips from the same production batch called in the following, microchip 6, 7 and 8, were prepared according to the same

Table 4
Maximal number of theoretical plates determined with Golay's plots as a function of film thickness. Values of half height width and efficiency were the average value obtained from 3 injections, and the RSD values are provided in brackets.

Microchip number	PDMS concentration ($mg.mL^{-1}$)	d_f (μm)	Retention factor (*k*) isooctane- (80 °C)	Maximal number of theoretical plates	E %
3	1	0.032	0.12	45,900 (10 %)	42 %
4	4	0.130	0.39	29,000 (2.1 %)	35 %
5	8	0.260	0.93	19,900 (1.6 %)	31 %

Table 5
B and C terms of the Golay's equation as a function of film thickness.

Microchip number	d_f (μm)	Longitudinal diffusion (B term)($\mu m.s^{-1}$)	Mass transfer C term) (s)
3	0.032	7.10^7	1.10^{-4}
4	0.130	7.10^7	$1.7.10^{-4}$
5	0.260	7.10^7	$2.3.10^{-4}$

Table 6
Number of theoretical plates measured on batch 3 microchips with the injection of isooctane at 80 °C at a linear gas velocity of 60 $cm.s^{-1}$. The efficiency values were the average of 5 injections, and all RSD values were <5 %. The global RSD of the 3 microchip efficiency values was 4.8 %.

Microchip number	Number of theoretical plates
6	17,085
7	17,730
8	16,110

Table 7
Average retention factors of batch 3 microchips for each *n*-alkane with a single microchip injection of *n*-alkane mixture at 120 °C and at a linear gas velocity of 60 $cm.s^{-1}$ and the corresponding RSD values.

Alkane	$k_{average}$	RSD(k) %
C_8	0.7	2.4
C_9	1.9	2.1
C_{10}	4.5	2.0
C_{11}	10.2	2.2

protocol and using the same conditions (400 mbar evaporation rate and 0.260 μm film thickness) to evaluate the process repeatability.

The efficiencies of the microchips were very close (Table 6), and retention factors measured with *n*-alkanes (Table 7) were similar between tested microchips, with an RSD lower than 3 %. Results were comparable to those obtained for microchip 5 prepared with another batch. The chromatogram of *n*-alkane separation is shown in Fig. 12. These results demonstrated the repeatability of the microchip coating method.

The stationary phase stability was evaluated over 240 days by periodic injection of isooctane (Fig. 13). A slight decrease of k factor was observed demonstrating a good stationary phase stability.

5. Conclusion

The aim of this work was to adapt and optimize a static coating method applied for microchips designed for space exploration applications and integrated onto a robust fluidic interface with removable capillary connections and limited high temperature (150 °C). First, extra-column variances were minimized during chromatographic tests of coated microchips using a commercial chromatographic system. In particular, a small liner internal diameter (1.2 mm), a high data acquisition frequency (100 Hz) and an internal diameter geometry of capillary connections (100 μm) were selected.

Additionally, a stationary phase coating on these microchips was successfully performed using the conventional static method adapted with a lower temperature (150 °C) and reduced pressure (400 mbar). Reducing the coating velocity allowed an increase the efficiency by 100 %. Moreover, the efficiency measured varies from about 45,000 theoretical plates for the thinnest film (0.032 μm), to 19,900 plates for the thickest film (0.260 μm), and the retention is linearly correlated to the film thickness. Finally, the repeatability of the process was evaluated. The efficiency and retention of three identically coated microchips were shown to be reproducible with a thick film of 0.260 μm. The film thickness can then be selected according to the volatility and polarity of the target compounds being analyzed, but when using a column length of only five meters, a greater film thickness could be better to separate complex mixtures as expected during space exploration missions.

In the future, we plan to use our microchips for *in situ* exploration missions to study planetary environments. For this the effect of the temperature variation on the stationary phase stability, during cruise flight or spatial mission, will be investigated. An immobilized and higher-temperature-resistance stationary phase will also be coated on a microchip for a longer life-time during space missions. Further work carried out by our team on the separation of more complex mixtures and their comparison with conventional columns used on space GCs will also be discussed.

CRediT authorship contribution statement

Arnaud Philippart: Writing – original draft, Methodology, Formal analysis. **Valérie Peulon-Agasse:** Writing – review & editing, Validation, Supervision, Conceptualization. **Malak Rizk-Bigourd:** Writing – review & editing, Writing – original draft, Validation, Supervision, Project administration, Methodology. **Audrey Boco-Simon:** Writing – review & editing, Validation. **Gabin Bergerot:** Writing – review & editing, Data curation. **Guillaume Rioland:** . **Arnaud Buch:** Writing – review & editing, Visualization, Methodology, Conceptualization. **Cyril Szopa:** Writing – review & editing, Validation, Supervision, Funding acquisition, Conceptualization. **Pascal Cardinael:** Writing – review & editing, Supervision, Project administration, Methodology, Funding acquisition, Data curation, Conceptualization.

Declaration of competing interest

The authors declare the following financial interests/personal relationships which may be considered as potential competing interests:

Pascal Cardinael reports financial support was provided by French Space Agency. Arnaud Philippart reports financial support was provided by Normandy Region. Arnaud Philippart reports financial support was provided by French Space Agency. Valerie Agasse reports financial support was provided by French Space Agency. Malak Rizk-Bigourd reports financial support was provided by French Space Agency. Audrey Boco-Simon reports financial support was provided by French Space Agency. Gabin Bergerot reports financial support was provided by French Space Agency. Guillaume Rioland reports financial support was provided by French Space Agency. Arnaud Buch reports financial support was provided by French Space Agency. Cyril Szopa reports financial support was provided by French Space Agency. Phillipart has patent #Patent FR2315012 pending to assignee. Boco-simon has patent #Patent FR2315012 pending to assignee. Agasse has patent #Patent FR2315012 pending to assignee. Szopa has patent #Patent FR2315012 pending to assignee. Buch has patent #Patent FR2315012 pending to assignee. Cardinael has patent #Patent FR2315012 pending to assignee.

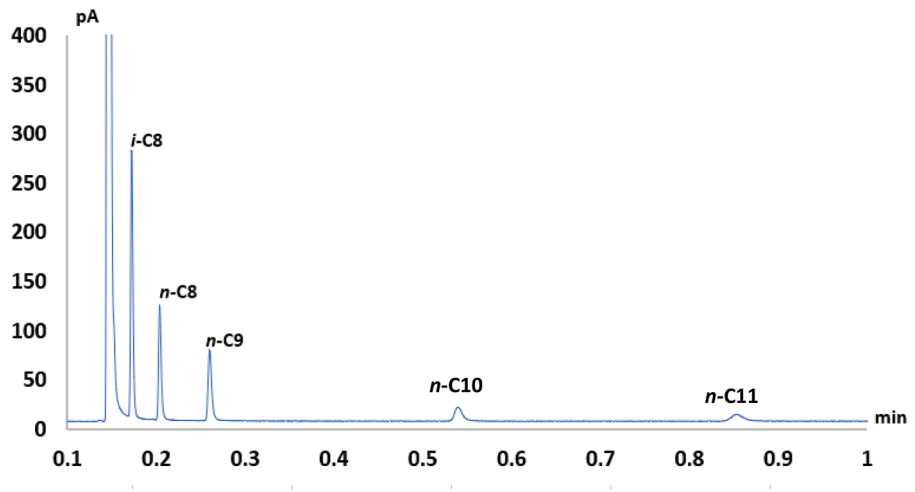

Fig. 12. Chromatogram obtained with microchip 6 for a mixture of *n*-alkane (isooctane (*i*-C8), octane (*n*-C8), nonane (*n*-C9), decane (*n*-C10) and undecane (*n*-C11) with pentane (*n*-C5) as solvent; the concentration of each *n*-alkane is 10 µL.mL^{-1}) at a linear gas velocity of 60 cm.s^{-1} and an isotherm oven temperature of 120 °C.

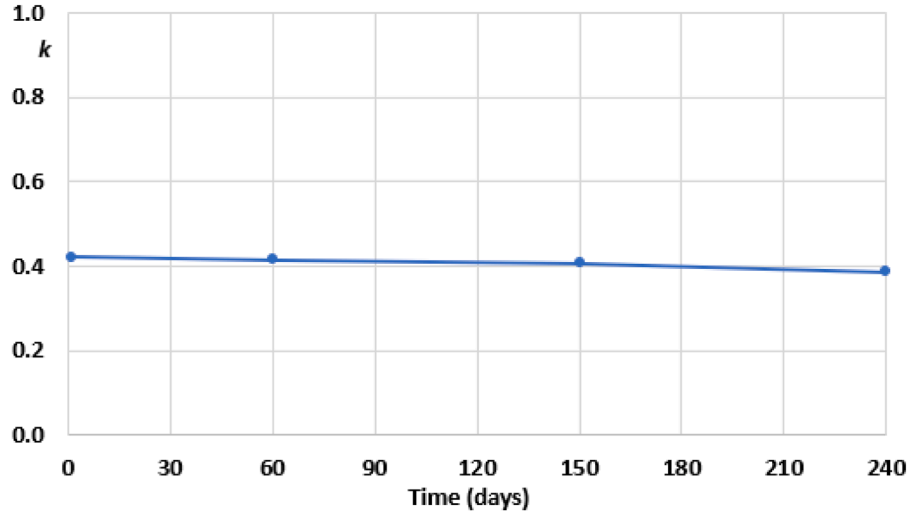

Fig. 13. Evolution of retention factor of isooctane (average of 5 injections without measurable deviation) measured at 80 °C on microchip 6 as a function of time.

Rizk-Bigourd has patent #Patent FR2315012 pending to assignee. If there are other authors, they declare that they have no known competing financial interests or personal relationships that could have appeared to influence the work reported in this paper.

Data availability

Data will be made available on request.

Acknowledgments

This work was supported by the CNES (Centre national d'études spatiales, Toulouse), which facilitates the project "R&T GC-MEMS" involving GC column miniaturization for space exploration and by the "Region Normandy". Both provided funding for the development of the columns, the laboratory experiments, and the PhD grant of A. Philippart, first author of this article.

References

[1] M. Millan, C. Szopa, A. Buch, P. Coll, D.P. Glavin, C. Freissinet, R. Navarro-Gonzalez, P. François, D. Coscia, J.Y. Bonnet, S. Teinturier, M. Cabane, P. R. Mahaffy, In situ analysis of martian regolith with the SAM experiment during the first mars year of the MSL mission: identification of organic molecules by gas chromatography from laboratory measurements, Planet. Space Sci. 129 (2016) 88–102, https://doi.org/10.1016/j.pss.2016.06.007.

[2] P.R. Mahaffy, C.R. Webster, M. Cabane, P.G. Conrad, P. Coll, S.K. Atreya, R. Arvey, M. Barciniak, M. Benna, L. Bleacher, W.B. Brinckerhoff, J.L. Eigenbrode, D. Carignan, M. Cascia, R.A. Chalmers, J.P. Dworkin, T. Errigo, P. Everson, H. Franz, R. Farley, S. Feng, G. Frazier, C. Freissinet, D.P. Glavin, D.N. Harpold, D. Hawk, V. Holmes, C.S. Johnson, A. Jones, P. Jordan, J. Kellogg, J. Lewis, E. Lyness, C.A. Malespin, D.K. Martin, J. Maurer, A.C. McAdam, D. McLennan, T. J. Nolan, M. Noriega, A.A. Pavlov, B. Prats, E. Raaen, O. Sheinman, D. Sheppard, J. Smith, J.C. Stern, F. Tan, M. Trainer, D.W. Ming, R.V. Morris, J. Jones, C. Gundersen, A. Steele, J. Wray, O. Botta, L.A. Leshin, T. Owen, S. Battel, B. M. Jakosky, H. Manning, S. Squyres, R. Navarro-González, C.P. McKay, F. Raulin, R. Sternberg, A. Buch, P. Sorensen, R. Kline-Schoder, D. Coscia, C. Szopa, S. Teinturier, C. Baffes, J. Feldman, G. Flesch, S. Forouhar, R. Garcia, D. Keymeulen, S. Woodward, B.P. Block, K. Arnett, R. Miller, C. Edmonson, S. Gorevan, E. Mumm, The sample analysis at mars investigation and instrument suite, Space Sci. Rev 170 (2012) 401–478, https://doi.org/10.1007/s11214-012-9879-z.

[3] K. Biemann, J.L. Bada, Comment on "Reanalysis of the Viking results suggests perchlorate and organics at midlatitudes on Mars" by Rafael Navarro-González et al, J. Geophys. Res. 116 (2011) E12001, https://doi.org/10.1029/2011JE003869.

[4] A. Ghosh, C.R. Vilorio, A.R. Hawkins, M.L. Lee, Microchip gas chromatography columns, interfacing and performance, Talanta 188 (2018) 463–492, https://doi.org/10.1016/j.talanta.2018.04.088.

[5] E. Lussac, R. Barattin, P. Cardinael, V. Agasse, Review on micro-gas analyzer, systems: feasibility, separations and applications, Crit. Rev. Anal. Chem 46 (2016) 455–468, https://doi.org/10.1080/10408347.2016.1150153.

[6] B.P. Regmi, M. Agah, Micro gas chromatography: an overview of critical components and their integration, Anal. Chem. 90 (2018) 13133–13150, https://doi.org/10.1021/acs.analchem.8b01461.
[7] F. Haghighi, Z. Talebpour, A. Sanati-Nezhad, Through the years with on-a-chip gas chromatography: a review, Lab. Chip 15 (2015) 2559–2575, https://doi.org/10.1039/C5LC00283D.
[8] I. Azzouz, J. Vial, D. Thiébaut, R. Haudebourg, K. Danaie, P. Sassiat, J. Breviere, Review of stationary phases for microelectromechanical systems in gas chromatography: feasibility and separations, Anal. Bioanal. Chem. 406 (2014) 981–994, https://doi.org/10.1007/s00216-013-7168-7.
[9] G. Lambertus, A. Elstro, K. Sensenig, J. Potkay, M. Agah, S. Scheuering, K. Wise, F. Dorman, R. Sacks, Design, fabrication, and evaluation of microfabricated columns for gas chromatography, Anal. Chem. 76 (2004) 2629–2637, https://doi.org/10.1021/ac030367x.
[10] J.H. Sun, H.Y.Cai D.F.Cui, X. Chen, L.L. Zhang, H. Li, J.H. Sun, H.Y.Cai D.F.Cui, X. Chen, L.L. Zhang, H. Li, Advanced gas chromatography - progress in agricultural, biomedical and industrial applications, IntechOpen (2012) 51–66.
[11] J. Crucello, A.M. de Oliveira, N.M.F.M. Sampaio, L.W. Hantao, Miniaturized systems for gas chromatography: developments in sample preparation and instrumentation, J. Chromatogr. A. 1685 (2022) 463603, https://doi.org/10.1016/j.chroma.2022.463603.
[12] X. Sun, J. Shi, X. Men, Y. Li, H. Qu, Y. Chang, J. Hu, X. Yan, W. Guo, C. Sun, DuanMicrochip gas chromatography column using magnetic beads coated with polydimethylsiloxane and metal organic frameworks, J. Chromatogr. A 1705 (2023) 464188. Article.
[13] M.V. Russo, G. Goretti, Soriero Preparation and application of fused-silica capillary microcolumns (25-50 μm ID) in gas chromatography, Ann. Chim. 86 (1996) 115–124.
[14] R. Haudebourg, J. Vial, D. Thiebaut, K. Danaie, J. Breviere, P. Sassiat, I. Azzouz, B. Bourlon, Temperature-programmed sputtered micromachined gas chromatography columns: an approach to fast separations in oilfield applications, Anal. Chem. 85 (2013) 114–120, https://doi.org/10.1021/ac3022136.
[15] R.C. Blase, M.J. Libardoni, G.P. Miller, K.E. Miller, C.M. Phillips-Lander, C.R. Glein, J.H. Waite, A. Ghosh, A. Venkatasubramanian, M.W. Li, A. Stephens, X. Fan, K. Kurabayashi, MEMS GC column performance for analyzing organics and biological molecules for future landed planetary missions, Front. Astron. Space Sci. 9 (2022) 828103, https://doi.org/10.3389/fspas.2022.828103.
[16] R.C. Blase, M.J. Libardoni, G.P. Miller, K.E. Miller, C.M. Phillips-Lander, J. H. Waite, C.R. Glein, H. Zhu, A. Ghosh, A. Venkatasubramanian, X. Fan, K. Kurabayashi, Experimental coupling of a MEMS gas chromatograph and a mass spectrometer for organic analysis in space environments, ACS Earth Space Chem 4 (2020) 1718–1729, https://doi.org/10.1021/acsearthspacechem.0c00131.
[17] R.C. Blase, M.J. Libardoni, C.R. Glein, K.E. Miller, J.H. Waite, M.W. Li, K. Kurabayashi, X. Fan, Biosignature detection from amino acid enantiomers with portable gas chromatography systems, Adv. Devices Instrum. 5 (2024) 0049, https://doi.org/10.34133/adi.0049.
[18] J. Dziuban, A. Ǵrecka-Drzazga, K. Malecki, L. Nieradko, J. Mŕz, M. Szczygielska, Silicon components for gas chromatograph, Proceedings of SPIE - The International Society for Optical Engineering 4516 (2001) 249–257.
[19] M. Rizk-Bigourd, D. Coscia, F. Ferreira, P. Cardinael, C. Szopa, A. Buch, V. Agasse-Peulon, A., Boco-Simon, A. Philipart, Développement d'un prototype de chromatographe en phase gazeuse à base de composants de technologie MEMS (Micro-Electro-Mechanical System) couplant un pré-concentrateur d'échantillon/injecteur à désorption thermique, une colonne séparative et un détecteur à conductivité thermique. December 22, 2023, Patent FR2315012.
[20] Malak Rizk-Bigourd, Cyril Szopa, David Coscia, Jean-Pierre Pineau, Vincent Guerrini, Frederic Ferreira, Fabrice Bertrand, Arnaud Philippart, Audrey Boco, Guillaume Rioland, Valérie Peulon-Agasse, Arnaud Buch, Pascal Cardinael, Development and integration of an ultraminiaturized gas chromatograph prototype based on lab-on-a-chip microelectromechanical systems for space exploration missions, ACS Earth and Space Chem. 8 (2024) 1745–1756, https://doi.org/10.1021/acsearthspacechem.4c00111.
[21] A. Meziani, S. Verloy, O. Ferroukhi, S. Roca, A. Curat, S. Tisse, V. Peulon-Agasse, H. Gardeniers, G. Desmet, P. Cardinael, Evaluation of gas chromatography columns with radially elongated pillars as second-dimension columns in comprehensive two-dimensional gas chromatography, Anal. Chem. 94 (2022) 14126–14134, https://doi.org/10.1021/acs.analchem.2c01264.
[22] S. Reidy, G. Lambertus, J. Reece, R. Sacks, High-performance, static-coated silicon microfabricated columns for gas chromatography, Anal. Chem. 78 (2006) 2623–2630, https://doi.org/10.1021/ac051846u.
[23] A. Wang, S. Hynynen, A.R. Hawkins, S.E. Tolley, H.D. Tolley, M.L. Lee, Axial thermal gradients in microchip gas chromatography, J. Chromatogr. A 1374 (2014) 216–223, https://doi.org/10.1016/j.chroma.2014.11.035.
[24] A. Ghosh, J.E. Johnson, J.G. Nuss, B.A. Stark, A.R. Hawkins, L.T. Tolley, B. D. Iverson, H.D. Tolley, M.L. Lee, Extending the upper temperature range of gas chromatography with all-silicon microchip columns using a heater/clamp assembly, J. Chromatogr. A 1517 (2017) 134–141, https://doi.org/10.1016/j.chroma.2017.08.036.
[25] A.D. Radadia, R.D. Morgan, R.I. Masel, M.A. Shannon, Partially buried microcolumns for micro gas analyzers, Anal. Chem. 81 (2009) 3471–3477, https://doi.org/10.1021/ac8027382.
[26] C. Szopa, M. Cabane, P. Coll, D. Coscia, A. Buch, S. Teinturier, R. Navarro-Gonzalez, J.-P. Goutail, C. Montaron, J.-B. Rigal, P. Poinsignon, V. Guerrini, M.-S. Clerc, M. Meftah, L. Soldani, F. Mettetal, M. Jerôme, C. Philippon, A. Galic, J. Sablairolles, S. Triqueneaux, D. Chazot, B. Toffolo, F.Y. Rakoto, A. Gaboriaud, P. Mahaffy, Gas-chromatographic analysis of mars soil samples with the SAM instrument onboard Curiosity - the 180 first sols, in: European Planetary Science Congress 2013, London, United Kingdom 8, 2013 pp EPSC2013-870.
[27] F. Goesmann, W.B. Brinckerhoff, F. Raulin, W. Goetz, R.M. Danell, S.A. Getty, S. Siljeström, H. Mißbach, H. Steininger, R.D. Arevalo, A. Buch, C. Freissinet, A. Grubisic, U.J. Meierhenrich, V.T. Pinnick, F. Stalport, C. Szopa, J.L. Vago, R. Lindner, M.D. Schulte, J.R. Brucato, D.P. Glavin, N. Grand, X. Li, F.H.W. van Amerom, The Mars Organic Molecule Analyzer (MOMA) Instrument: characterization of organic material in martian sediments, Astrobiology 17 (2017) 655–685, https://doi.org/10.1089/ast.2016.1551.
[28] J.W. Barnes, E.P. Turtle, M.G. Trainer, R.D. Lorenz, S.M. MacKenzie, W. B. Brinckerhoff, M.L. Cable, C.M. Ernst, C. Freissinet, K.P. Hand, A.G. Hayes, S. M. Hörst, J.R. Johnson, E. Karkoschka, D.J. Lawrence, A.L. Gall, J.M. Lora, C. P. McKay, R.S. Miller, S.L. Murchie, C.D. Neish, C.E. Newman, J. Núñez, M. P. Panning, A.M. Parsons, P.N. Peplowski, L.C. Quick, J. Radebaugh, S.C.R. Rafkin, H. Shiraishi, J.M. Soderblom, K.S. Sotzen, A.M. Stickle, E.R. Stofan, C. Szopa, T. Tokano, T. Wagner, C. Wilson, R.A. Yingst, K. Zacny, S.C. Stähler, Science goals and objectives for the dragonfly titan rotorcraft relocatable lander, Planet. Sci. J. 2 (2021) 655–685, https://doi.org/10.3847/PSJ/abfdcf.
[29] S.C. Terry, J.H. Jerman, J.B. Angell, A gas chromatographic air analyzer fabricated on a silicon wafer, IEEE Trans Electron Devices 26 (1979) 1880–1886, https://doi.org/10.1109/T-ED.1979.19791.
[30] G. Wiranto, M.R. Haskard, D.E. Mulcahy, D.E. Davey, E.F. Dawes, Microengineered open tubular columns for GC analysis, Proceedings 3891 (1999) 168–177, https://doi.org/10.1117/12.364435.
[31] M. Agah, J.A. Potkay, G. Lambertus, R. Sacks, K.D. Wise, High-performance temperature-programmed microfabricated gas chromatography columns, J. of Microelectromechanical Systems 14 (2005) 1039–1050, https://doi.org/10.1109/JMEMS.2005.856648.
[32] V.R. Reid, R.E. Synovec, High-speed gas chromatography: the importance of instrumentation optimization and the elimination of extra-column band broadening, Talanta 76 (2008) 703–717, https://doi.org/10.1016/j.talanta.2008.05.012.
[33] C. Cagliero, S. Galli, M. Galli, I. Elmi, M. Belluce, S. Zampolli, B. Sgorbini, P. Rubiolo, C. Bicchi, Conventional and enantioselective gas chromatography with microfabricated planar columns for analysis of real-world samples of plant volatile fraction, J. Chromatogr. A 1429 (2016) 329–339, https://doi.org/10.1016/j.chroma.2015.12.037.
[34] S. Jespers, S. Schlautmann, H. Gardeniers, W.D. Malsche, F. Lynen, G. Desmet, Chip-based multicapillary column with maximal interconnectivity to combine maximum efficiency and maximum loadability, Anal. Chem. (2017) 11605–11613, https://doi.org/10.1021/acs.analchem.7b03036.